Exploration of Multitemporal COSMO-SkyMed Data via Interactive Tree-Structured MRF Segmentation

Raffaele Gaetano, Donato Amitrano, Giuseppe Masi, Giovanni Poggi, Giuseppe Ruello, *Member, IEEE,* Luisa Verdoliva, *Member, IEEE,* and Giuseppe Scarpa, *Member, IEEE*

Abstract—We propose a new approach for remote sensing data exploration, based on a tight human–machine interaction. The analyst uses a number of powerful and user-friendly image classification/segmentation tools to obtain a satisfactory thematic map, based only on visual assessment and expertise. All processing tools are in the framework of the tree-structured MRF model, which allows for a flexible and spatially adaptive description of the data. We test the proposed approach for the exploration of multitemporal COSMO-SkyMed data, that we appropriately registered, calibrated, and filtered, obtaining a performance that is largely superior, in both subjective and objective terms, to that of comparable noninteractive methods.

Index Terms—Classification, human–machine interaction, Markov random fields (MRF), multitemporal data, segmentation, synthetic aperture radar.

I. INTRODUCTION

THE constellations of sensors available nowadays provide data with unprecedented spatial resolution and revisit time. Therefore, the bulk of available data reached a level that can be hardly managed by human operators, leading to an extreme automation of algorithms, with techniques that alienate more and more the users from direct data management and analysis [1]–[3]. This paradigm, certainly necessary and advantageous in the data acquisition and storage steps, has been also extended to the data processing realm, leaving the user with the role of mere interpreter of results obtained through "black-boxes" implemented on the basis of some necessarily simplified models [4]. In remote sensing, this can lead to the misclassification of objects and the misidentification of phenomena, and eventually to a wrong interpretation of the data.

These problems can be mitigated by restoring the central role of the user as the key actor in a number of high-level decisional tasks. As brilliantly argued in [5], human beings and computer algorithms are good at solving different and mostly complementary tasks. As the interpreter cannot be asked to compute important data statistics and synthetic features, essential for all decision making processes, algorithms cannot be expected to

make correct decisions in a wide range of unpredictable situations, which arise quite often in remote sensing and cannot be taken into account by compact mathematical models. To obtain the most from the available data, the user must be given the opportunity to *interact* with the computer, in a simple and easily understood way, to drive the decision process. In such a way, due to real-time actions and reactions, the processing can be transformed from an "objective coding of the image information content" [6] into a machine learning process guided by the user's knowledge and judgment.

In this paradigm, the computer is only a flexible (yet powerful) number-crunching tool driven by the expert toward a solution that is *context-aware*, as opposed to the *context-independent* solutions offered by totally automatic processes, where by "context" we mean the many possible data peculiarities and specific application needs which call for dedicated work flows. The user–machine interaction is fundamental for recognizing the inconsistencies between the technique/model and the context in which it is applied, and the user becomes the central actor of this task, participating actively in the processing chain, based on the accumulated expertise [6].

Among the many image processing tasks relevant for remote sensing, segmentation is probably the one which could benefit most from the interactive paradigm described above. Although it is not obvious, in general, how to manage the huge amount of data provided by remote sensing, and what workflow is best suited to extract the information of interest from them [7], segmentation is very likely to be part of it. In [5], a model for remote-sensing data exploration is proposed. Not surprisingly, segmentation is taken as a running example to prove its potential, adopting a number of tools, under the user supervision, to extract a meaningful thematic map based on high resolution optical data and a digital elevation model of the scene. Following this seminal paper, recent work has focused on a more formal definition of the human–machine interaction frameworks and their applications to remote-sensing data analysis [6], [8]. The tendency to leverage user interaction in this domain is further confirmed by very recent works both in the SAR [9] and optical [10] context.

In this work, inspired by [5], we propose an innovative user-driven approach for the unsupervised land-cover classification of multitemporal COSMO-SkyMed SAR images. SAR image processing, especially in the multitemporal case, is a perfect example of the added value represented by the user intervention in the processing chain. Interpreting SAR images requires, in general, a deep understanding of many relevant physical processes and models. Moreover, with multitemporal data, the physical parameters of the scene vary not only in space but also in time, often

in an unpredictable way, affected by human activities which can induce both temporal patterns and local anomalies in the electromagnetic response. These circumstances can be controlled and mitigated interactively by the user who can modify the processing flow using available prior knowledge or information drawn from different sources.

In the proposed work flow, after the suitable preparation of data, we combine the multitemporal stack of intensities and the coherence maps extracted from it to obtain an accurate thematic map. Unlike in [5], most of the segmentation tools belong to a single flexible algorithmic suite, the Tree-Structured Markov Random Field (TS-MRF) algorithm, based on the model of the same name, originally proposed for the unsupervised [11], [12] and supervised [13] land-cover classification of multispectral images. Indeed, with its hierarchical nature, TS-MRF represents a natural basis for interactive segmentation, allowing the user to check and then validate, or further process, results that are confined to a single class or region of the image, without interfering with satisfactory results observed elsewhere. Moreover, the opportunity to work in a single algorithmic framework (without precluding the use of others, of course) reduces the training required of the users to take full advantage of the image processing and data analysis tools available. TS-MRF does not need training data (in unsupervised mode), hence is especially suited to data exploration. Its effectiveness has been largely proven in the segmentation of optical remote sensing data, while its application to SAR imagery has been long prevented only by the lack of data reliable enough for a detailed segmentation, a problem now overcome due to the wealth of multitemporal SAR data provided by the COSMO-SkyMed constellation. Human–machine interaction represents the correct modality to find a meeting point between challenging SAR-related tasks and well-founded and long-proven methods developed in the optical domain.

In Sections II and III, we briefly review the related work on MRF-based SAR data analysis, and the TS-MRF model and segmentation algorithm. Then, we describe the case study and available data, in Section IV, the data preprocessing phase, in Section V, and the actual exploration experiment in Section VI. Section VII provides a performance assessment, in both subjective and objective terms. Finally, Section VIII draws conclusions.

II. RELATED WORK

SAR image segmentation is an extremely challenging task. Beside, the mentioned need for a knowledge-based interpretation of phenomena, meaningful information must be extracted from data that exhibit a very high dynamics, and are characterized by speckle which severely corrupts region boundaries and fine details, preventing the use of classical image processing tools. In order to deal with speckled images, most of the segmentation techniques proposed in the literature adopt a Markov Random Field (MRF) approach [14]–[17]. By defining explicitly the spatial interaction between neighboring pixels, one can enforce suitable regularity constraints, avoiding so the highly fragmented segmentation output maps typical of pixel-level approaches.

Many variations to the classical MRF-based data-flow have been proposed as, e.g., embedding the MRF model in the clustering space and using graph cuts to search the optimal data clusters [2], or using a hierarchical MRF for multiresolution segmentation, with suitable expedients to avoid block artifacts [18]. Irrespective of the detail, all these methods are based on the assumption of a multiplicative noise with circular Gaussian statistics, which makes full sense for fully developed speckle. For high resolution SAR images, however, this model is not always appropriate, because it cannot be assumed that a large number of scatterers fall in any resolution cell, especially in urban areas. This observation has spawned a number of recent papers. In [19], a new model for the statistics of the scattering process is proposed, and used to improve the classification of urban areas. Another way to deal with high resolution images goes through the use of statistical learning methods with appropriate local descriptors. In [20], texture features are included in the MRF model to identify distinct ice types. In [21], a hierarchical Markov "aspect" model is proposed to generate dense and efficient terrain-class labeling by exploiting both high-level context and multiscale features. In [22], conditional random fields are used to incorporate context interactions in the extracted features. Clearly, for all these methods, a significant training phase is required.

All the methods outlined above have been proposed for a single intensity or amplitude SAR image. However, co-registered multitemporal SAR images provide a much richer information, with new opportunities for land-cover classification. First of all, they allow one to use effective despeckling filters, improving significantly the quality of data. Despeckling has never been a popular option for the segmentation of single-look images, because of a possible resolution loss (mostly absent, though, in modern despeckling techniques [23], [24]). With multitemporal data available, however, undue smoothing effects can be avoided altogether. Needless to say, despeckling modifies data statistics, and models for unfiltered data do not apply anymore. Of course, beside the improved data quality, the mere fact that a *vector* of data is associated with each pixel opens the way to major improvements in segmentation and classification. Indeed, with their very high spatial resolution combined with a short revisit time these data represent a powerful tool for accurate interpretation of the ground scene. Therefore, in recent years, research has focused mostly on application-oriented tasks rather then methodological developments: supervised land-cover classification [25], urban-area segmentation [26], [27], flood mapping [28], flood monitoring [29], [30], and wet snow cover in a mountainous area [31]. A major advantage in using a multitemporal stack for classification stems from the intrinsic ability to deal with classes that exhibit a peculiar temporal behavior, allowing to extract information about, e.g., seasonal changes and periodic land use. Moreover, new mixed classes, due to changes in the scene, e.g., after a fire or a landslide, may be detected as well, since the affected area will exhibit a separable response vector. These transition areas, difficult to characterize without prior information on when the event occurred, especially benefit from the interactive approach proposed in this work, which allows for a posterior annotation supported by user knowledge (e.g., photo-interpretation aided by optical data).

We conclude this short review of the literature by mentioning the method recently proposed in [32], where the binary partition trees [33] are used to perform the hierarchical segmentation of multidimensional SAR data. A multiple-resolution description of the image is obtained, with a structured representation which supports easy access and processing of subsets of regions. Although not based on MRF models, this method performs SAR image segmentation through a hierarchical approach, similar in principle to the one used here. This is not surprising, though, since the hierarchical approach fits very well the scale-dependent and non-stationary nature of SAR images.

III. THE TS-MRF SUITE FOR INTERACTIVE CLASSIFICATION

In this section, we recall briefly the principles of TS-MRF image modeling, and define the related elementary actions for unsupervised segmentation which are combined to obtain the final segmentation map. This combination, and hence the detailed processing chain, was fully automated in the original TS-MRF algorithm, while here it is the user that selects at each time the actions most suitable for the data exploration goal. We refer the reader to [12], [13], and [34] for a more detailed description.

A. The TS-MRF Model

In the TS-MRF model, the image, defined on the set of sites $\mathcal{S}$, with observable data y, is associated with a binary unbalanced tree. Each node t of the tree is associated with a region (not necessarily connected) $\mathcal{S}^t$ of the whole image, and hence with the corresponding data y^t. To each *internal* node, a label map x^t is also associated which, for each pixel $s \in \mathcal{S}^t$ can assume only two values $x_s^t \in \{t^{\text{left}}, t^{\text{right}}\}$ pointing at the two children nodes. Therefore, the label map of node t defines the regions associated with its children nodes $\mathcal{S}^{\text{left}} = \{s \in \mathcal{S}^t : x_s^t = t^{\text{left}}\}$ and $\mathcal{S}^{\text{right}} = \{s \in \mathcal{S}^t : x_s^t = t^{\text{right}}\}$. The root is associated with the whole image $(\mathcal{S}, y)$, and its binary label map divides the image in two non-overlapping regions. Proceeding recursively, each internal node/region is further partitioned, until the K leaves of the tree are reached which, collectively, partition the whole image in K disjoint regions.

To this structural model, we now add a statistical model. Each label map is modeled as a binary Markov random field (MRF), with distribution $p(x^t) = \Pr(X^t = x^t)$, while the observable at the leaves are modeled as multivariate Gaussian variables $y_s^t \sim N(\mu^t, \mathbf{C}^t)$ independent on one another given the label. As a consequence, the observables in the internal nodes are mixtures of Gaussian. However, they can also be approximated as Gaussian if detailed information on the nodes is lacking (unsupervised case). In this tree-structured model, a dedicated binary MRF is associated locally with each node/region, which allows to adapt accurately to the non-stationary behavior typical of images. The non-stationarity is indeed *the* major issue in image modeling, and certainly the major limit of "flat" MRF models. TS-MRF modeling is a powerful method to address this problem.

B. TS-MRF Segmentation

Given the above model, the TS-MRF recursive segmentation is readily described. The fundamental action is the so called *node*

splitting, while further actions, the *merge-split refinement*, and the *topological split* allow to improve overall accuracy.

1) Node Splitting: For each node t, a binary MRF segmentation is carried out according to the *Maximum a Posteriori* (MAP) criterion

$$\widehat{x}^t = \arg\max_{x^t} p(x^t|y^t) = \arg\max_{x^t} p(y^t|x^t)p(x^t). \quad (1)$$

Therefore, $\widehat{x}^t$ is the most probable label map given the observables and the MRF prior at the node. Although any binary MRF prior can be adopted at the nodes, the classical Potts model is preferred for the sake of simplicity, and class parameters are estimated with a Maximum Likelihood (ML) approach. If no prior information is available (general unsupervised case), segmentation and class-wise parameters are jointly computed in a Estimation-Minimization (EM) fashion, by iteratively performing ML (given the class membership) and MAP (given the model parameters) estimation. Refer to [12] and [35] for further details.

In the supervised case [13], a significant prior knowledge is supposed to be available, due to preliminary data exploration or other sources of information. In particular, the structure of the tree is known in advance, and hence the number of leaves K, corresponding to the number of classes. Moreover, the parameters μ^t, C^t are supposed to be known for each class, and therefore all node likelihoods $p(y^t)$ are also perfectly known. In this setting, the only matter is the solution of the binary segmentation problems (1). In the unsupervised case [12], instead, all information must be estimated for each node. This includes the tree structure itself, and the number of leaves. In [12], this latter problem is solved by using an indicator, computed locally for each node, the split gain, which drives the growth of the tree by indicating at any time which leaf must be split and providing a stopping condition. Obviously, lacking any annotation of the source data, the meaning of each region singled out is not provided, and the task of associating regions to semantic classes is left to the user. It is worth underlining that, for a given number of classes, TS-MRF segmentation is computationally lighter than flat MRF segmentation.

2) Merge-Split Refinement: The exclusive use of *binary* splits represents a constraint which might impair the segmentation performance, because of the inability of the algorithm to deal with non-binary structures. In [12], a new action was added to address this problem, the merge-split refinement.

The example in Fig. 1 illustrates a typical over-segmentation problem due to the binary constraint. Part (a) shows a synthetic image with three distinct regions, x, y, and z. In some infortunate cases, due to region statistics, the first binary split may produce a segmentation, like in part (b), where region y is split between nodes 2 and 3. The further split of these nodes will produce the final 4-class segmentation of part (c), where two different nodes, 5 and 6, correspond to two adjacent parts of the same region y, a clear failure of the algorithm.

This over-segmentation problem is solved by introducing, after each split, a merge-split phase. Each newly created child node is tentatively merged with each of the other nodes, except the sibling, and then split again based on a local binary MRF.
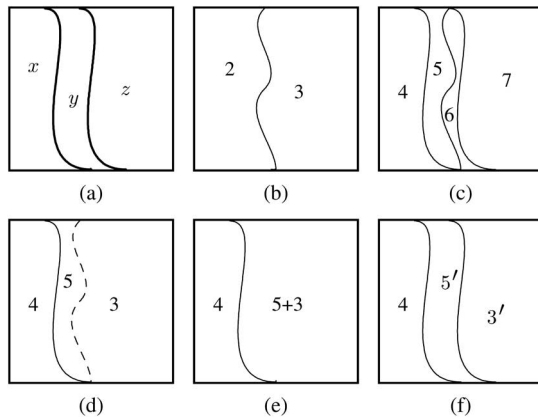
Fig. 1. Merge-split refinement: (a) ground truth, (b) initial binary split, (c) final 4-class segmentation without refinement, (d) intermediate 3-class segmentation, refinement by (e) merging and (f) binary split.

Fig. 2. Google Earth view of the study area. The covered area is approximately $15 \text{ km} \times 13 \text{ km}$.

For each tested merge-split, a merging gain is computed. Eventually, the merge-split with the largest gain (if positive) is validated. The overall effect of this action is a refinement of the boundary between the two involved nodes. In the bottom part of Fig. 1, we illustrate the effect of one such merge-split action. After the splitting of node 2, we have nodes 4, 5, and 3, in part (d); the merging of nodes 5 and 3, in part (e), reassembles the over-segmented region y, while the subsequent split of the merged node $(5 + 3)$, in part (f), provides the desired segmentation.

3) Topological Split: Another important action was introduced in [34]. The segmentation carried out by TS-MRF is clearly class-oriented. However, if the user is interested in segmentation in a more strict sense, rather than classification, there is no point in keeping a single class-wise data description, as it represents only a constraint which can impair local accuracy. In fact, separate segments belonging to the same class can have quite different statistics, especially with large and noisy images.

Therefore, when TS-MRF is used in the context of pure segmentation, aimed at building an object-level description of the image, after each binary split a topological split of the children classes follows, in which disjoint segments are assigned different labels. Each MRF split, which generates always two children nodes, is therefore followed by a topological split, which can be void, if the class is already connected, but more often generates a very large number of children. Of course, the huge increase in the number of nodes has a significant cost in terms of computational burden. On the other hand, a description of the data local to each segment cannot but improve the accuracy of subsequent binary MRF splits.

The elementary actions described above were proposed originally for automatic segmentation, driven by suitable numerical indicators, such as the split gain, the merge gain, and other node statistics. Here, they will be given to the user as basic tools, to be used interactively on the basis of a continuous inspection of results.

IV. CASE STUDY AND DATA

Our case study concerns the province of Caserta, in southern Italy, between the Volturno river and the Regi Lagni artificial channel (reference coordinates are $41°01'50''N, 13°59'04''E$).

The area, whose Google Earth view is shown in Fig. 2, is prevalently rural, with densely inhabited coastal settlements, and a flat topography. It includes cultivated fields, human settlements, large tanks, and small water harvesting facilities. Most of the fields are managed by family farms, so that the agricultural production units are very small (less than 4 hectares on average) and the terrain is cultivated with different plantations, each providing a different temporal feature in the radar reflectivity.

Fifteen COSMO-SkyMed stripmap SAR images are available, of size 5200×4600 pixels, spanning a temporal interval of 2 years, between December 14, 2009 and October 17, 2011. The data are HH polarized, acquired with ascending orbit and a look angle of approximately $33°$. Spatial resolution is 3 m, for an overall coverage of about 195 km^2.

Our aim is to recover the best possible range of land-cover information, in the absence of a ground truth, through the interactive segmentation of the whole area, driven by joint visual inspection of the SAR data and the corresponding optical view of the scene.

Fig. 3(a) shows a false-color representation of the scene, obtained using the intensities of three SAR images acquired in different seasons, April (red), August (green), and December (blue), 2010. In Fig. 4, we show some selected sections of this image and highlight some classes that might reasonably be found in a good thematic map. A "water" class (up-left) is clearly distinguishable from its low response at any season. Another "tanks" class (up-middle) comprises small agricultural tanks which are empty in the summer and filled in the other seasons, and appear in full green in our RGB composition. Pine groves and uncultivated crops are included in a "permanent vegetation" class (up-right) which has a fairly stable response throughout the year and hence appears close to gray in the image. Finally, we could identify three main types of crops, characterized by different seasonal behaviors, called "dry crops I," "dry crops II," and "wet crops," in the absence of more specific information, and shown in the bottom part of the figure.

Based on this set of classes, a ground truth was generated, shown in Fig. 3(b), by manually annotating several areas of the image. It is worth underlining that this ground truth was *not* used in any way during the interactive segmentation phase, but only at
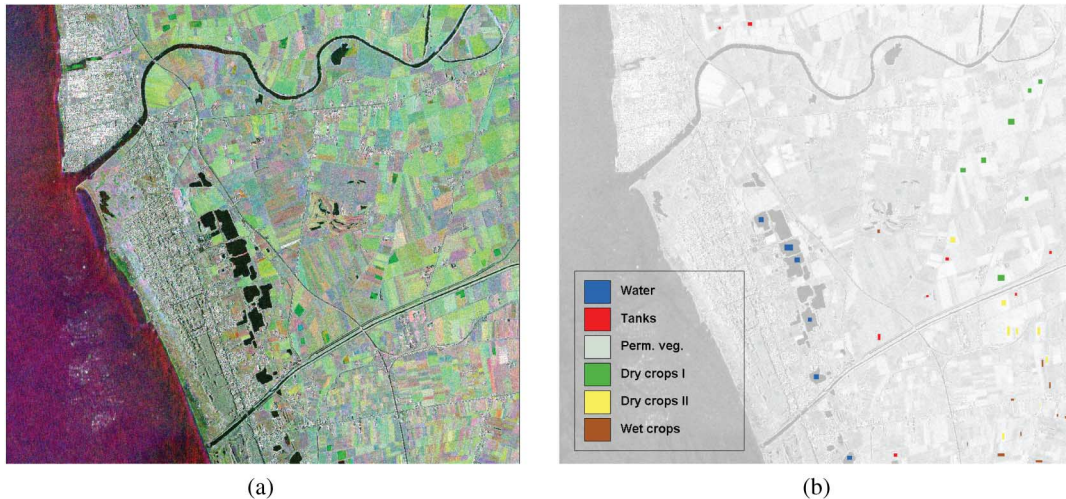
Fig. 3. False-color representation of the data (a) and selected ground truth (b).
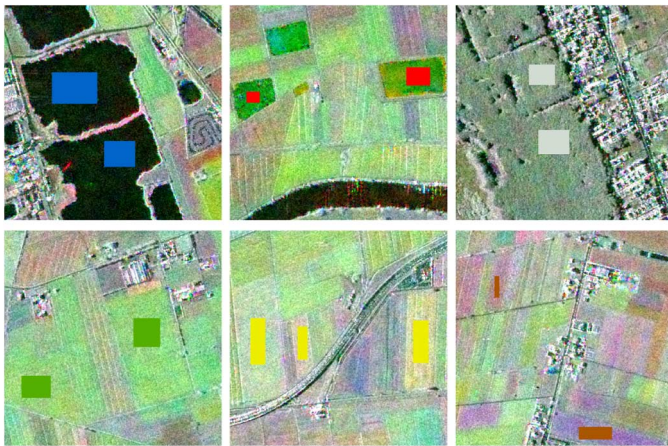
Fig. 4. Ground truth samples for the homogeneous classes (*water*, *tanks*, *permanent vegetation*, *dry crops I* and *II*, *and wet crops*).

TABLE I
DATASET SUMMARY

Acquisition date	Calib. coeff. [dB]
2009-12-14	−36.3176
2009-12-30	−36.9188
2010-01-15	−39.0413
2010-03-20	−40.7196
2010-04-05	−38.4177
2010-04-21	−40.1378
2010-08-11	−46.5234
2010-08-27	−41.1693
2010-09-12	−40.5112
2010-09-28	−39.4239
2010-12-17	−39.9272
2011-01-18	−40.0279
2011-02-03	−40.8033
2011-06-27	−46.9393
2011-10-17	−46.5963

a later stage for testing purposes, allowing us to compare the proposed method with suitable references in terms of classification accuracy.

A further "man-made" class is eventually considered, comprising the urban areas and other artificial structures. The urban areas, in particular, characterized by tiny details and a high response heterogeneity, cannot be easily identified based on the multitemporal vector of intensities. An expert could fairly easily find them based on textural properties which, however, are hardly captured by statistical models [36]. Here, we will resort to a further piece of information the average coherence, which is typically very large for stable artificial structures and much smaller otherwise.

V. DATA PREPARATION

In order to fully exploit the wealth of information provided by the COSMO-SkyMed data, using the TS-MRF suite with the smallest possible variations w.r.t. the optical image case, a number of preliminary processing steps are necessary:

1) spatial registration;
2) radiometric calibration;
3) despeckling;
4) homomorphic transform.

The data registration has been carried out via the three-step procedure proposed in [37]. After a coarse registration based on orbital data, a refinement based on correlation of amplitude data, and a final step based on coherence evaluation, the images are aligned with sub-pixel precision.

With multitemporal images, a meaningful comparison of data acquired in different dates requires a reliable calibration procedure. This step is of fundamental importance for a better visual inspection by the user. As explained in [38], COSMO-SkyMed Single Look Complex Balanced products are already corrected for effects related to the sensor and the acquisition geometry. Hence, the sigma naught can be evaluated by applying a calibration factor which can be computed from ancillary data. The list of the available product dates and the corresponding calibration factors are shown in Table I.

As mentioned in Section II, the availability of a number of co-registered images of the same scene, gives us the opportunity to significantly improve the data quality by a suitable despeckling. In the proposed processing chain, we apply an optimal weighting
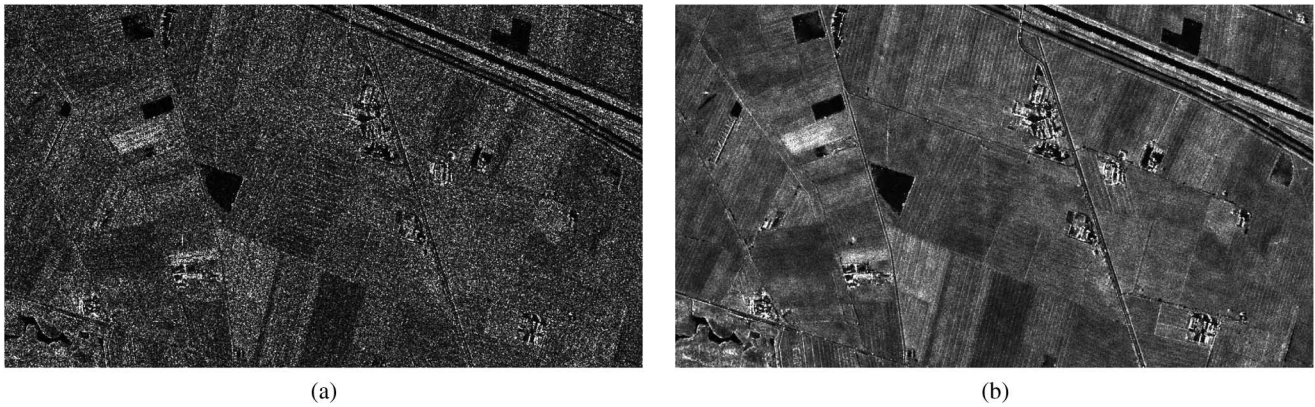
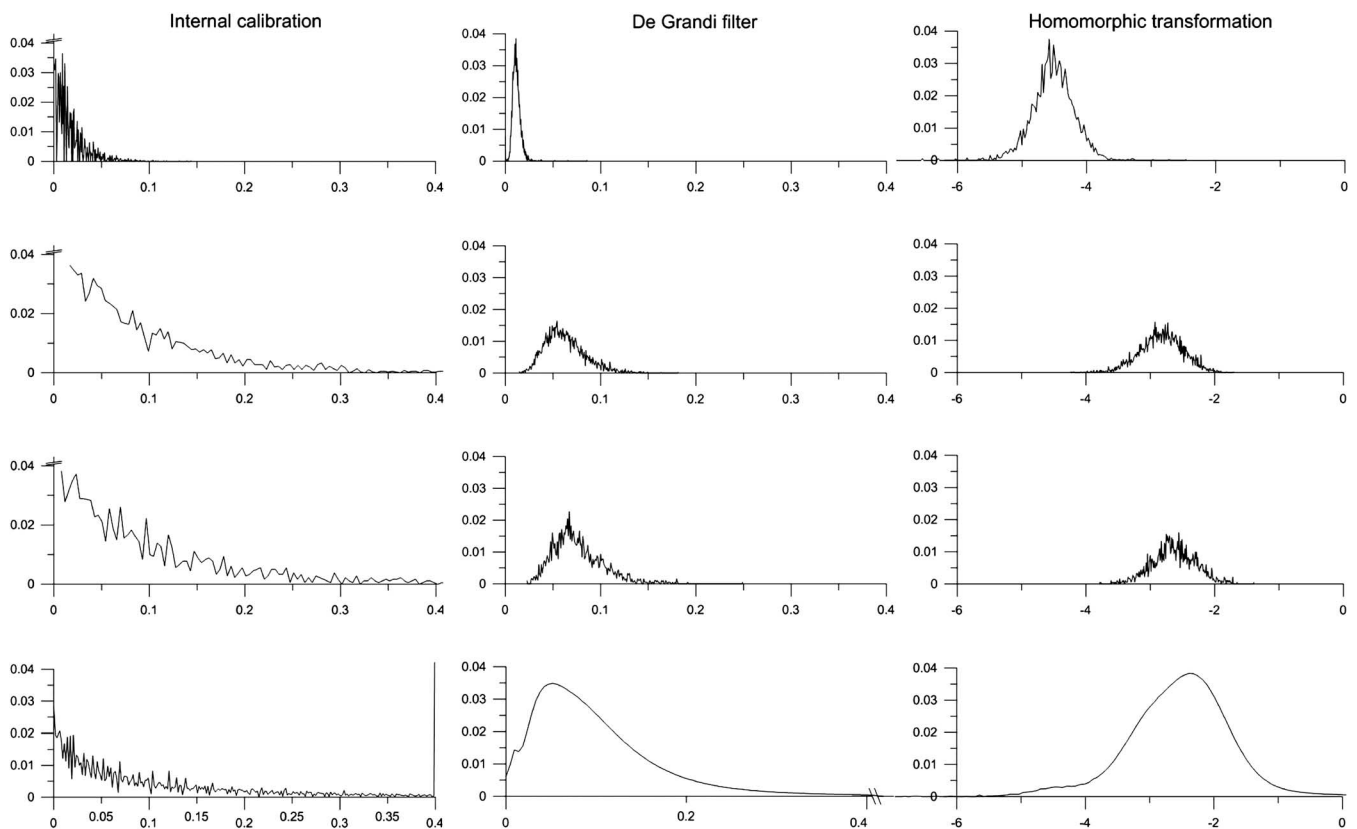Fig. 5. Comparison between SLC products before (a) and after (b) the application of the De Grandi filter.

Fig. 6. Variation of the image statistics along the processing chain for different classes (water, permanent vegetation, and crops) and for the whole scene, from top to bottom.

De Grandi filter [39] which allows a speckle reduction in the order of 12 equivalent number of looks, without any loss in spatial resolution. In Fig. 5, we show a subset of the 2010-04-05 image together with its despeckled version: the quality improvement is obvious, as well as the preservation of spatial resolution.

At this processing stage, data intensities do not follow anymore an exponential statistic (if they ever did before despeckling) but they are certainly not Gaussian, not even approximately. On the other hand, TS-MRF relies on the hypothesis that data are Gaussian, conditionally on the class they belong to. Therefore, in order to apply the TS-MRF suite without any structural modification, we

perform a point-wise homomorphic transformation of the data, which provides class-wise statistics of the scene much closer to the Gaussian distributions. It goes by itself that, even after this processing, this is still only a convenient approximation, but this holds just as well for optical images. More important is the fact that the class-wise distributions show a negligible skewness, allowing us to proceed as usual with second-order statistics.

To provide some more insight into the effects of these operations, Fig. 6 shows a number of data distributions observed at various stages of the processing chain, for the 2010-04-05 image. In all cases, we report the frequency of occurrence of
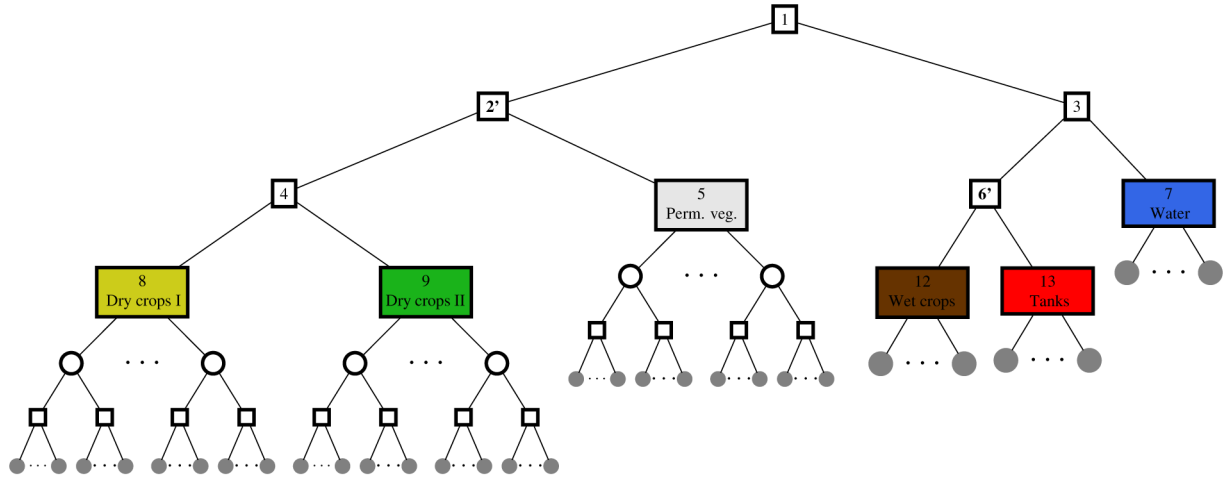
Fig. 7. TS-MRF tree evolution: squared nodes come from binary MRF splits; circular nodes come from topological splits; prime superscript indicate a class obtained by merge-split refinement; filled circles represent elements of the object layer.

observations as a function of the intensity, using always the same scale on both x- and y-axis to enable an easy comparison. In particular, the distributions are computed after internal calibration (first column), after despeckling (middle column), and after logarithmic rescaling (last column). The first three rows show class-wise statistics for the water, permanent vegetation, and a crop class, respectively, while the last row concerns the whole image.

As expected, despeckling modifies significantly the statistics observed in homogeneous areas, which pass from the characteristic exponential distribution of the SLC intensity product to a more symmetric one. The homomorphic transform, eventually, leads to distributions that are reasonably well fit by Gaussians.

Note that, while the water class is clearly separable from the other two, these latter have distributions that overlap significantly. However, the permanent vegetation has a fairly stable response during all the year, contrary to the crops, where the response is significantly influenced by state of the cultivations. By exploiting information on the whole time series, these two classes can be easily separated as well.

VI. INTERACTIVE TS-MRF-BASED SEGMENTATION

We now describe the interactive segmentation of our multi-temporal SAR stack carried out with the tools provided by the TS-MRF suite. As explained in Section III, the user can select at any moment one of the following three actions:

1) split;
2) split-and-merge refinement;
3) topological split.

Since our aim is land-cover classification, we consider only the first two actions, initially, leaving the third one for the final stage when we build an object layer used to recover the man-made class.

In automatic TS-MRF algorithm, the choice on whether to split some nodes, and in which order, is based on a locally computed split gain parameter. In interactive mode, instead the user assesses by visual inspection the meaningfulness of any split to decide whether to proceed, validating the split, or to stop. After

TABLE II
SUMMARY OF USER ACTIONS (FINAL CLASSES IN BOLD)

	Action	Node	Emerging Classes	
Classification	Node splitting	Root	2	*Dry*
			3	*Dry + wet*
	Node splitting	3	6	*Semi-wet + dry*
			7	**Water**
	Merge-split Ref.	2,6	2'	*Dry*
			6'	*Semi-wet*
	Node splitting	6'	12	**Wet crops**
			13	**Tanks**
	Node splitting	2'	4	*Dry crops*
			5	**Perm. vegetation**
	Node splitting	4	8	**Dry crops I**
			9	**Dry crops II**
Obj. L.	Topological split	*Dry* leaves (8,9,5)	-	

each class split, the newly created classes can be compared with the other ones to check whether a merging is needed. Again, in the automatic version of the algorithm, a specific parameter, the merging gain, is used to drive this process. In the interactive mode, this decision is left to the user responsibility. In general, merge-split refinement should not be abused, resorting to it only when one of the children classes is clearly over-segmented, with complementary parts dropped into another class.

In our experiment, we obtained fairly naturally the six-class segmentation tree shown in Fig. 7 (stopping at the colored nodes) using only visual information on class homogeneity and region compactness. The colors have been set only afterward, by optimizing the matching of the selected classes with the ground-truth classes. Note that only one merging was actually required to prevent over-segmentation. Such refinement affected the nodes labeled as 2' and 6', obtained by means of a suitable reshaping of the original classes labeled 2 and 6. More specifically, such reshape eventually helped recovering the integrity of class 12 ("wet crops"), eventually anchored to 6'. A full summary of the user actions is reported in Table II, together with the classes emerging at each step of the process.
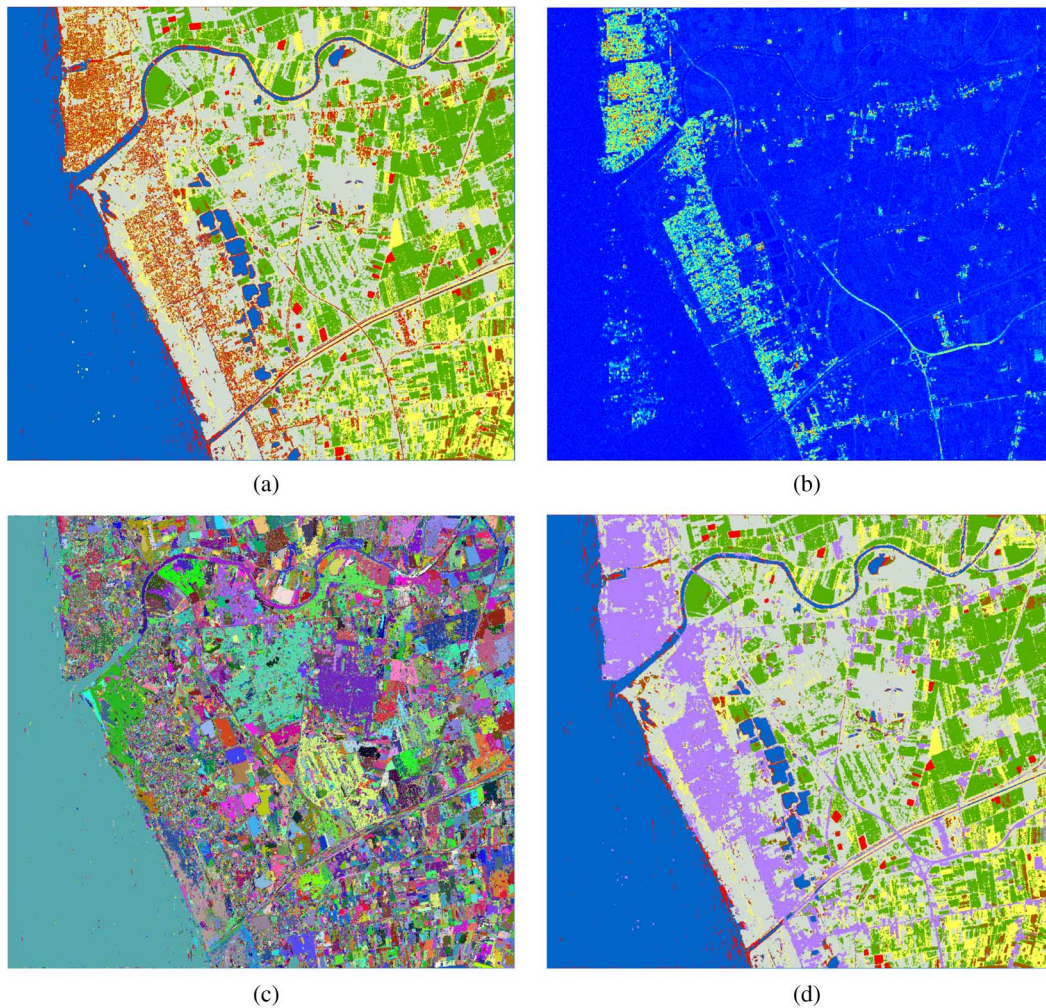
Fig. 8. Segmentation products. (a) 6-class TS-MRF classification. (b) Low-resolution coherence map. (c) Full object-layer. (d) Final 7-class segmentation.

Fig. 8(a) shows the segmentation map associated with our 6-class tree. This result, however interesting, is obviously incomplete, as it lacks a dedicated man-made class. Indeed, the presence of some areas characterized by a significant class variability can be noticed in the map. These areas correspond mainly to urban settlements, characterized by very fine details, therefore they cannot fall into any of the above classes, but parts of them are retrieved in all six of them.

To single out man-made regions, we resort to the coherence map, shown in Fig. 8(b), obtained by averaging the pair-wise coherence of the oldest with all the others images. In fact, built-up areas exhibit typically a high coherence, which seems to be confirmed in our experiment. A simple way to obtain a reasonable man-made class is by thresholding the coherence map. By so doing, however, very irregular areas would be eventually extracted, and many inland artificial structures would be lost, especially the thin roads, due to the lower resolution of the coherence map. Such inconveniences can be avoided by resorting again of the TS-MRF suite. By applying a topological split to all classes, and then a further MRF split of

each new segment, followed by a final topological split, a new tree is obtained, with terminal nodes (filled circles in Fig. 7) which correspond to elementary connected components of the map. The set of all these components forms an "object layer," that is a higher-level representation of the image opposed to the pixel-level, shown in Fig. 8(c) for our case study. We then perform thresholding at object-level rather than at pixel-level, featuring each object with its average coherence value. This very simple solution, which strongly relies on the available segmentation and hence constitutes a byproduct of the interactive classification, provides a much more consistent and accurate man-made class, shown in lilac in the final output map in Fig. 8(d) together with the other six original classes, properly reshaped. Note that, since the coherence information is projected on the original high-resolution objects, no loss of details is observed, and tiny structures are faithfully preserved. Note also that segments generated by the topological split of classes in the right part of the tree ("water," "tanks," and "wet crops") do not need a further MRF split since they are already quite homogeneous, hence we skip this last step for such segments.
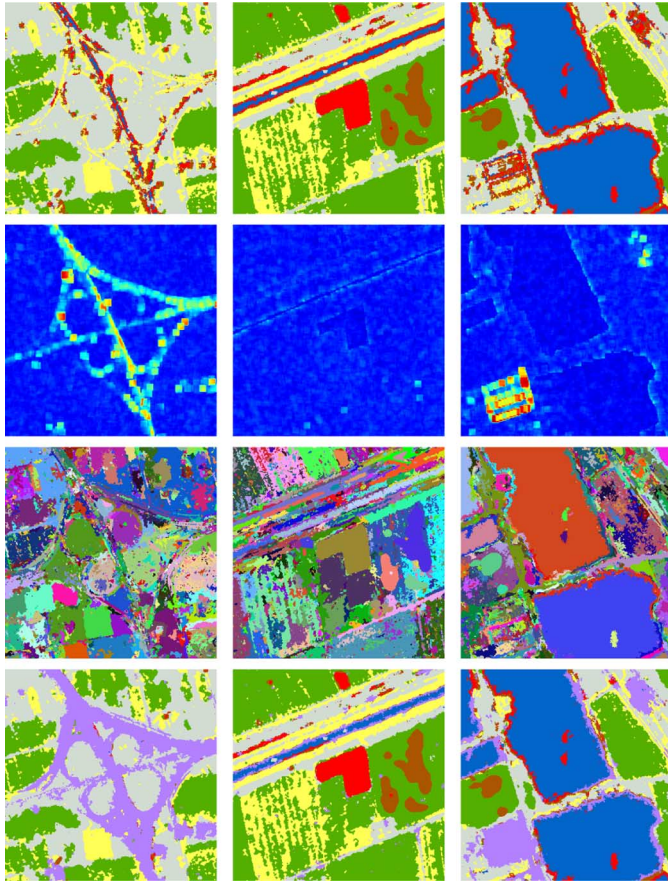
Fig. 9. Close-ups from Fig. 8. From top to bottom: 6-class map, coherence, object layer, 7-class map.

VII. PERFORMANCE ASSESSMENT

Visual inspection of the 7-class map in Fig. 8(d) seems to confirm the potential of the proposed TS-MRF-based technique for interactive segmentation. The most relevant regions of interest have been clearly extracted, with a good level of detail up to the finest scales, as confirmed by the close-ups shown in Fig. 9. Of course, the quality of the SAR data used in this experiment, in terms of both spatial resolution and number of observations, plays a fundamental role in such good results. Nonetheless, the obtained performance seems much superior to that of conventional techniques working on the very same data.

In Fig. 10(a) and (b), we show the 6-class segmentation maps obtained by using a "flat" (non tree-structured, noninteractive) MRF-based segmentation, both in unsupervised and supervised modality, to be compared with the analogous 6-class map in Fig. 8(a) (obviously, the man-made class, based on external features, is not considered in this comparison). To train the supervised segmenter, we used a fraction of the ground truth in Fig. 3(b) as training set (around 35% of the area for each class), leaving the rest as test set for numerical evaluation. In Tables III–V, we report the confusion matrices computed on the test set for

unsupervised MRF, supervised MRF, and interactive TS-MRF, respectively.

The unsupervised classifier scores very poorly in terms of overall accuracy, $\tau = 56.18\%$. With its balanced approach, given only the number of classes as prior information, it tends to the refinement of the classes with the higher data variability, missing altogether several others. The supervised classifier, as expected, performs much better, achieving an overall accuracy $\tau = 81.82\%$. Interactive TS-MRF significantly outperforms both, with 87.22% of correctly classified pixels. These results were not at all obvious in advance. Remember that the proposed classifier is, in the usual sense, unsupervised, i.e., it makes no use of prior information available on the classes of interest. The user can only decide which nodes to split, and possibly merge again, but has no influence on the binary local segmentations. Under this point of view, the most correct reference for the proposed approach is indeed the unsupervised MRF, and the huge performance gain speaks volumes about the importance of human/computer interaction.

Nonetheless, we observe a considerable gain also w.r.t. the supervised classifier. Looking in detail at the two confusion matrices, we note that in both cases the "water" and "tanks" classes have been almost perfectly recovered due to their distinctive features. Significant differences arise instead on several vegetation classes. The poor performance of the supervised classifier on the permanent vegetation class is likely due to its strong inner variability, which can be hardly captured by a single multivariate Gaussian distribution. In the interactive approach, this class is identified by exclusion, after several other classes have been already well defined, hence it suffer less from over-segmentation. The "wet crops" class, instead, is a smaller class very local to the image, which is well recovered in the interactive case mainly due to the merge-split refinement performed in early stages. In summary, the observed gain is probably due to the better class-adaptivity of the tree-structured model, together with the opportunity of exploiting it through the user intervention.

For the man-made class, we limit the assessment to a suitable visual inspection of the result. In Fig. 11, we compare, for various thresholds, a section of the man-made class obtained working at pixel-level (top) and at object-level (bottom) using the object layer provided by interactive TS-MRF. At all thresholds, the object-based class appears to be less noisy, and to better preserve the shape of the component regions. Moreover, in the pixel-based solution, the variation of the threshold changes rather gracefully the level of noise in the map, providing little clues on which threshold best tradesoff noise against the preservation of important details. With the object-based solution, instead, by varying the threshold, entire objects of the scene appear/disappear, allowing for an easier selection of the "correct" level according to the highlighted content.

One might argue that a better man-made class could be obtained through a direct contextual segmentation of the coherence map. However, Fig. 12 clearly shows that this is not the case. Next to a detail of the original continuous-valued coherence map (a), we show its binary segmentation obtained with the MRF
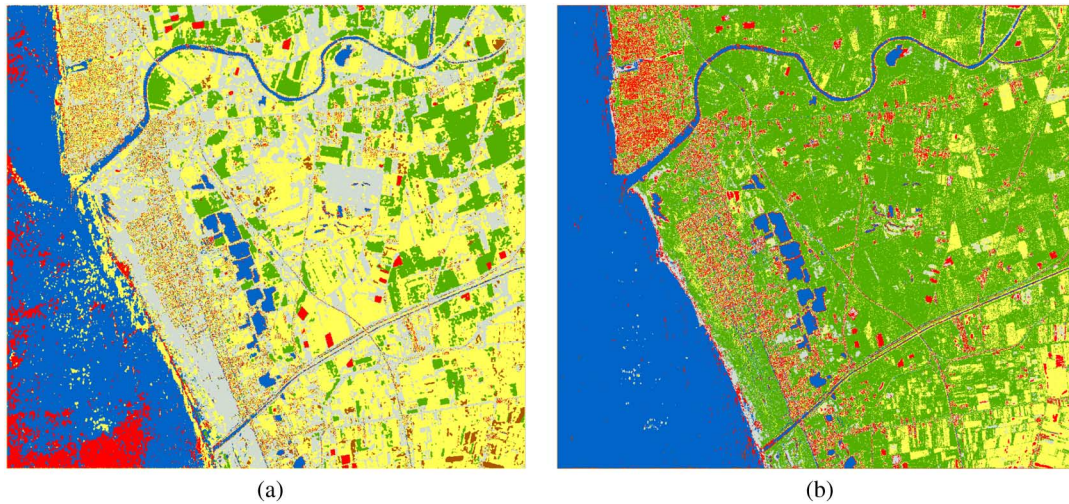
Fig. 10. Thematic maps obtained using the supervised (a) and unsupervised (b) flat MRF classification.

TABLE III
CONFUSION MATRIX FOR THE UNSUPERVISED FLAT MRF-BASED CLASSIFIER. IN BOLD, PER-CLASS CORRECTLY CLASSIFIED PIXELS AND OVERALL ACCURACY

	Water	Tanks	Perm. Veg.	Dry Crops I	Dry Crops II	Wet Crops	User acc.
Water	**8516**	0	16	0	0	0	99.81%
Tanks	54	**3444**	11	0	0	1402	70.13%
Perm. Veg.	1	1231	**888**	253	33	338	32.36%
Dry Crops I	0	0	6215	**4334**	649	833	36.02%
Dry Crops II	0	0	1527	4721	**7614**	1977	48.07%
Wet Crops	51	29	0	0	0	**0**	0%
Prod. acc.	98.77%	73.21%	10.26%%	46.56%	91.78%	0%	$\tau = $ **56.18%**

TABLE IV
CONFUSION MATRIX FOR THE SUPERVISED FLAT MRF-BASED CLASSIFIER. IN BOLD, PER-CLASS CORRECTLY CLASSIFIED PIXELS AND OVERALL ACCURACY

	Water	Tanks	Perm. Veg.	Dry Crops I	Dry Crops II	Wet Crops	User acc.
Water	**8541**	0	0	0	0	0	100%
Tanks	55	**4636**	0	23	0	0	98.35%
Perm. Veg.	1	0	**4465**	0	0	639	87.46%
Dry Crops I	5	0	3	**9187**	740	0	92.47%
Dry Crops II	20	68	3893	98	**7495**	2124	54.72%
Wet Crops	0	0	296	0	61	**1787**	83.35%
Prod. acc.	99.06%	98.55%	51.58%%	98.70%	90.34%	39.27%	$\tau = $ **81.82%**

TABLE V
CONFUSION MATRIX FOR THE INTERACTIVE TS-MRF-BASED CLASSIFIER. IN BOLD, PER-CLASS CORRECTLY CLASSIFIED PIXELS AND OVERALL ACCURACY

	Water	Tanks	Perm. Veg.	Dry Crops I	Dry Crops II	Wet Crops	User acc.
Water	**8515**	0	0	0	0	0	100%
Tanks	107	**4704**	0	0	0	0	97.78%
Perm. Veg.	0	0	**6260**	0	0	654	90.54%
Dry Crops I	0	0	1980	**8721**	918	538	71.74%
Dry Crops II	0	0	101	2	**7378**	440	93.14%
Wet Crops	0	0	316	585	0	**2918**	76.41%
Prod. acc.	98.76%	100%	72.31%	93.69%	88.93%	64.13%	$\tau = $ **87.22%**

model of Section III-B1 (b), and the result obtained by object-based thresholding (c). Direct MRF segmentation suffers the obvious problems related to the low-resolution original data: most thin details are lost due to excessive regularization, and even large objects exhibit less continuity where coherence values are less dense. This last example underlines the potential offered by the object-layer, and hence by the low-level segmentation, for SAR data exploration.
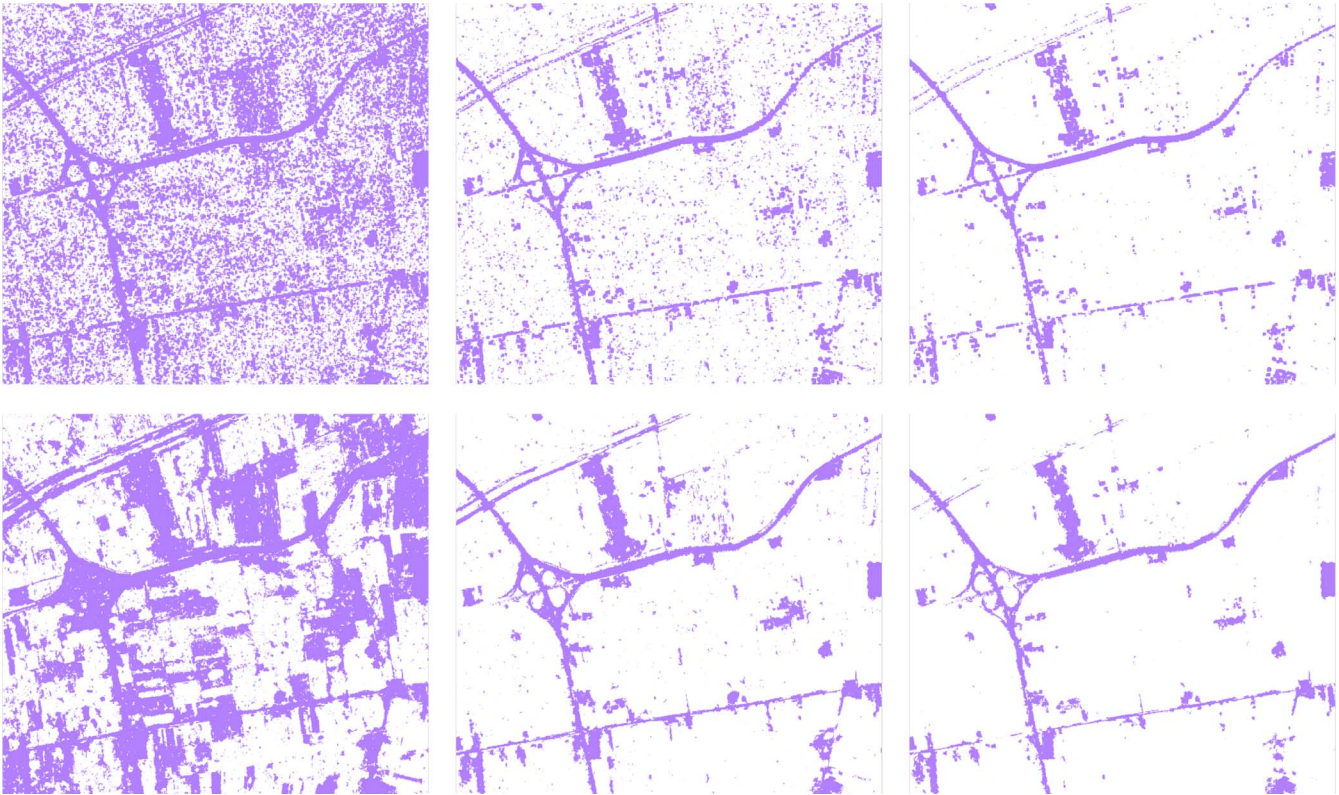
Fig. 11. Pixel layer vs. object layer man-made class extraction. Top: maps obtained through pixel-level thresholding of the coherence map, with thresholds 0.15, 0.18, and 0.21. Bottom: maps obtained through object-level thresholding at the same levels.
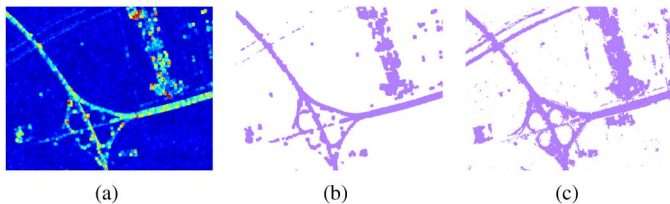

| (a) | (b) | (c) |

Fig. 12. Direct contextual segmentation of the coherence map vs. object-based thresholding. (a) Detail of the coherence map. (b) MRF segmentation. (c) Object-based thresholding.

VIII. CONCLUSION

Fundamental tasks in remote-sensing data analysis, such as segmentation and classification, cannot be easily automated and hence require some forms of supervision to provide satisfactory results. Traditionally, supervision comes in the form of some statistical description of the object/classes found in the scene, through a preliminary analysis, and the collection of training data. In this work, with reference to the challenging case of multitemporal high-resolution SAR data, we show that much better results can be obtained by following an interactive data exploration paradigm. Here, no prior analysis is required, but the user can perform simple actions, based on prior knowledge and experience, that guide the process toward the most satisfactory results.

This approach, of course, rests upon the availability of powerful and easy-to-use basic tools. We show that the TS-MRF algorithmic suite fits well this approach, and allows one to obtain very valuable results. The hierarchical image model, which adapts to the local statistics of the classes, provides the required flexibility to deal with non-standard problems. In the considered case study, the interactive use of TS-MRF allowed us to obtain a better thematic map than with a conventional supervised approach. Moreover, by leveraging on the object-layer made available by the suite, we could also accurately recover a high-definition man-made class.

Despite such good results, there is much room for improvements under many respects. In this work, we used a very limited set of possible actions, but many more can be conceived. Keeping the very promising hierarchical framework, more sophisticated MRF models can be used, possibly varying from node to node, possibly K-ary instead of binary. Other classes of models, alternative to the MRFs, can also be considered to deal with specific problems, such as the recovery of macro-textures, road networks, etc. We are already investigating some of these topics.

REFERENCES

[1] L.-K. Soh and C. Tsatsoulis, "Segmentation of satellite imagery of natural scenes using data mining," *IEEE Trans. Geosci. Remote Sens.*, vol. 37, no. 2, pp. 1086–1099, Mar. 1999.
[2] G.-S. Xia, C. He, and H. Sun, "A rapid and automatic MRF-based clustering method for SAR images," *IEEE Geosci. Remote Sens. Lett.*, vol. 4, no. 4, pp. 596–600, Oct. 2007.
[3] Y. Bazi, L. Bruzzone, and F. Melgani, "An unsupervised approach based on the generalized Gaussian model to automatic change detection in multitemporal SAR," *IEEE Trans. Geosci. Remote Sens.*, vol. 43, no. 4, pp. 874–887, Apr. 2005.

[4] R. N. Giere, "Using models to represent reality," in *Model-Based Reasoning in Scientific Discovery*, L. Magnani, N. J. Nersessian, and P. Thagard, Eds. New York, NY, USA: Springer-Verlag, 1999, pp. 41–57.

[5] V. Madhok and D. Landgrebe, "A process model for remote sensing data analysis," *IEEE Trans. Geosci. Remote Sens.*, vol. 40, no. 3, pp. 680–686, Mar. 2002.

[6] M. Datcu and K. Seidel, "Human centered concepts for exploration and understanding of satellite images," *IEEE Trans. Geosci. Remote Sens.*, vol. 43, no. 3, pp. 52–59, Oct. 2005.

[7] M. Schröder, H. Rehrauer, K. Seidel, and M. Datcu, "Spatial information retrieval from remote-sensing images—Part II: Gibbs-Markov random fields," *IEEE Trans. Geosci. Remote Sens.*, vol. 36, no. 5, pp. 1446–1455, Sep. 1998.

[8] D. Bratasanu, I. Nedelcu, and M. Datcu, "Interactive spectral band discovery for exploratory visual analysis of satellite images," *IEEE J. Sel. Topics Appl. Earth Observ. Remote Sens.*, vol. 5, no. 1, pp. 207–224, Feb. 2012.

[9] G. P. Bernad, L. Denise, and P. Réfrégier, "Hierarchical feature-based classification approach for fast and user-interactive SAR image interpretation," *IEEE Geosci. Remote Sens. Lett.*, vol. 6, no. 1, pp. 117–121, Jan. 2009.

[10] J. dos Santos, P.-H. Gosselin, S. Philipp-Foliguet, R. da S. Torres, and A. X. Falcao, "Interactive multiscale classification of high-resolution remote sensing images," *IEEE J. Sel. Topics Appl. Earth Observ. Remote Sens.*, vol. 6, no. 4, pp. 2020–2034, Aug. 2013.

[11] G. Poggi and R. Ragozini, "Image segmentation by tree-structured Markov random fields," *IEEE Signal Process. Lett.*, vol. 6, no. 7, pp. 155–157, Jul. 1999.

[12] C. D'Elia, G. Poggi, and G. Scarpa, "A tree-structured Markov random field model for Bayesian image segmentation," *IEEE Trans. Image Process.*, vol. 12, no. 10, pp. 1259–1273, Jan. 2003.

[13] G. Poggi, G. Scarpa, and J. Zerubia, "Supervised segmentation of remote sensing images based on a tree-structured MRF model," *IEEE Trans. Geosci. Remote Sens.*, vol. 43, no. 8, pp. 1901–1911, Aug. 2005.

[14] P. Kelly, H. Derin, and K. Hartt, "Adaptive segmentation of speckled images using a hierarchical random field model," *IEEE Trans. Acoust. Speech Signal Process.*, vol. 36, no. 10, pp. 1628–1641, Oct. 1988.

[15] E. Rignot and R. Chellappa, "Segmentation of polarimetric Synthetic Aperture Radar data," *IEEE Trans. Image Process.*, vol. 1, no. 3, pp. 281–300, Jul. 1992.

[16] A. S. Solberg, T. Taxt, and A. Jain, "A Markov random field model for classification of multisource satellite imagery," *IEEE Trans. Geosci. Remote Sens.*, vol. 34, no. 1, pp. 100–113, Jan. 1996.

[17] P. Smits and S. Dellepiane, "Synthetic Aperture Radar image segmentation by a detail preserving Markov random field approach," *IEEE Trans. Geosci. Remote Sens.*, vol. 35, no. 4, pp. 844–857, Jul. 1997.

[18] Y. Yang, H. Sun, and C. He, "Supervised SAR image MPM segmentation based on region-based hierarchical model," *IEEE Geosci. Remote Sens. Lett.*, vol. 3, no. 4, pp. 517–521, Oct. 2006.

[19] C. Tison, J.-M. Nicolas, F. Tupin, and H. Maitre, "A new statistical model for Markovian classification of urban areas in high-resolution SAR images," *IEEE Trans. Geosci. Remote Sens.*, vol. 42, no. 10, pp. 2046–2057, Oct. 2004.

[20] H. Deng and D. Clausi, "Unsupervised segmentation of synthetic aperture radar sea ice imagery using a novel Markov random field model," *IEEE Trans. Geosci. Remote Sens.*, vol. 43, no. 3, pp. 528–538, Mar. 2005.

[21] W. Yang, D. Dai, B. Triggs, and G. Xia, "SAR-based terrain classification using weakly supervised hierarchical Markov aspect models," *IEEE Trans. Image Process.*, vol. 21, no. 9, pp. 4232–4243, Sep. 2012.

[22] Y. Ding, Y. Li, and W. Yu, "SAR image classification based on CRFs with integration of local label context and pairwise label compatibility," *IEEE J. Sel. Topics Appl. Earth Observ. Remote Sens.*, vol. 7, no. 1, pp. 300–306, Jan. 2014.

[23] C. Deledalle, L. Denis, G. Poggi, F. Tupin, and L. Verdoliva, "Exploiting patch similarity for SAR image processing: the nonlocal paradigm," *IEEE Signal Process. Mag.*, vol. 31, no. 4, pp. 69–78, Jul. 2014.

[24] G. Di Martino, M. Poderico, G. Poggi, D. Riccio, and L. Verdoliva, "Benchmarking framework for SAR despeckling," *IEEE Trans. Geosci. Remote Sens.*, vol. 52, no. 3, pp. 1596–1615, Mar. 2014.

[25] L. Bruzzone, M. Marconcini, U. Wegmller, and A. Wiesmann, "An advanced system for the automatic classification of multitemporal SAR images," *IEEE Trans. Geosci. Remote Sens.*, vol. 42, no. 6, pp. 1321–1334, Jun. 2004.

[26] X. Niu and Y. Ban, "An adaptive contextual SEM algorithm for urban land cover mapping using multitemporal high-resolution polarimetric SAR data," *IEEE J. Sel. Topics Appl. Earth Observ Remote Sens.*, vol. 5, no. 4, pp. 1129–1139, Aug. 2012.

[27] J. Deng, Y. Ban, J. Liu, X. N. L. Li, and B. Zou, "Hierarchical segmentation of multitemporal RADARSAT-2 SAR data using stationary wavelet transform and algebraic multigrid method," *IEEE Trans. Geosci. Remote Sens.*, vol. 52, no. 7, pp. 4353–4363, Jul. 2014.

[28] S. Martinis and A. Twele, "A hierarchical spatio-temporal Markov model for improved flood mapping using multi-temporal X-band SAR data," *Remote Sens.*, vol. 2, pp. 2240–2258, 2010.

[29] S. Dellepiane, E. Angiati, and G. Vernazza, "Processing and segmentation of COSMO-SkyMed images for flood monitoring," in *Proc. IEEE Int. Geosci. Remote Sens. Symp.*, 2010, pp. 4807–4810.

[30] L. Pulvirenti, N. Pierdicca, M. Chini, and L. Guerriero, "Monitoring flood evolution in vegetated areas using COSMO-SkyMed data: The Tuscany 2009 case study," *IEEE J. Sel. Topics Appl Earth Observ. Remote Sens.*, vol. 6, no. 4, pp. 1807–1816, Aug. 2013.

[31] T. Schellenberger, B. Ventura, M. Zebisch, and C. Notarnicola, "Wet snow cover mapping algorithm based on multitemporal COSMO-SkyMed X-band SAR images," *IEEE J. Sel. Topics Appl. Earth Observ. Remote Sens.*, vol. 5, no. 3, pp. 1045–1053, Jun. 2012.

[32] A. Alonso-Gonzàlez, S. Valero, J. Chanussot, C. Lòpez-Martinez, and P. Salembier, "Processing multidimensional SAR and hyperspectral images with binary partition tree," *Proc. IEEE*, vol. 101, no. 3, pp. 723–747, Mar. 2013.

[33] P. Salembier and L. Garrido, "Binary partition tree as an efficient representation for image processing, segmentation, and information retrieval," *IEEE Trans. Image Process.*, vol. 9, no. 4, pp. 561–576, Jan. 2000.

[34] C. D'Elia, G. Poggi, and G. Scarpa, "Improved tree-structured segmentation of remote sensing images," in *Proc. IEEE Int. Geosci. Remote Sens. Symp.*, Aug. 2003, vol. 3, no. 1, pp. 1805–1807.

[35] A. Mohammad-Djafari, "Joint estimation of parameters and hyperparameters in a Bayesian approach of solving inverse problems," in *Proc. 3rd IEEE Int. Conf. Image Process.*, 1996, vol. 1, pp. 473–476.

[36] G. Scarpa, R. Gaetano, M. Haindl, and J. Zerubia, "Hierarchical multiple Markov chain model for unsupervised texture segmentation," *IEEE Trans. Image Process.*, vol. 18, no. 8, pp. 1830–1843, Aug. 2009.

[37] D. Amitrano, G. Di Martino, A. Iodice, D. Riccio, G. Ruello, M. N. Papa, F. Ciervo, and Y. Koussoube, "Effectiveness of high-resolution SAR for water resource management in low-income semi-arid countries," *Int. J. Remote Sens.*, vol. 35, no. 1, pp. 70–88, 2014.

[38] e-GEOS. *COSMO-SkyMed Image Calibration* [Online]. Available: http://www.e-geos.it/products/pdf/COSMO-SkyMed-Image_Calibration.pdf

[39] G. De Grandi, M. Leysen, J.-S. Lee, and D. Schuler, "Radar reflectivity estimation using multiple SAR scenes of the same target: Technique and applications," in *Proc. IEEE Int. Geosci. Remote Sens. Symp.*, 1997, pp. 1047–1050.

Raffaele Gaetano received the Laurea (M.S.) degree in computer engineering and the Ph.D. degree in electronic and telecommunication engineering, both from the University of Naples Federico II, Naples, Italy, in 2004 and 2009, respectively.

He has been a ERCIM Post-Doctoral Fellow of both the ARIANA team of INRIA Sophia Antipolis and the DEVA team of SZTAKI, Research Institute of the Hungarian Academy of Sciences. From 2010 to 2013, he has been a Post-Doctoral Fellow with the TELECOM ParisTech, Paris, France, within the MultiMédia Group. Currently, he is a Post-Doctoral Member of the Research Group on Image Processing (GRIP), Department of Electric and Information Technology Engineering, University of Naples Federico II. His research interests include the field of image and video analysis and processing, with interests ranging from color- and texture-based hierarchical image segmentation, morphological image analysis and object detection, mainly applied to the classification of remote sensing images, to image restoration, stereo vision, and image/video super-resolution.

Donato Amitrano was born in Naples, Italy, on December 27, 1985. He received the Bachelor's degree in aerospace engineering, the Master's degree in aerospace and astronautical engineering, in 2009 and 2012, respectively, and is currently pursuing the Ph.D. degree in electronic and telecommunication engineering all from the University of Naples Federico II, Naples, Italy.

In September 2012, he joined as a Graduate Researcher with the Department of Electrical Engineering and Information Technology, University of Naples Federico II. His research interests include multitemporal SAR, remote-sensing techniques for developing countries, SAR images interpretation, and data fusion.

Mr. Amitrano is an invited reviewer for some remote-sensing specialized journals such as IEEE TRANSACTIONS ON GEOSCIENCE AND REMOTE SENSING, *International Journal of Remote Sensing*, and *Remote Sensing Letters*.

Giuseppe Masi was born in Piedimonte Matese, Italy, on February 13, 1984. He received the Laurea (B.S.) and Laurea Magistrale (M.S.) degrees in electronic engineering (summa cum laude) from the University of Naples Federico II, Naples, Italy, in July 2012. Since March 2013, he has been pursuing the Ph.D. degree in electronic and telecommunication engineering from the University of Naples Federico II, within the Research Group on Image Processing (GRIP).

His research interests include the field of morphological image analysis and segmentation.

Giovanni Poggi received the Laurea (M.S.) degree in electronic engineering from the University of Naples Federico II, Naples, Italy, in 1988.

Currently, he is a Professor of Telecommunications with the same institution and Coordinator of the Telecommunication Engineering School. His research interests include statistical image processing, including compression, restoration, segmentation, and classification, with application to the area of remote-sensing, both optical and SAR, and digital forensics.

Prof. Poggi has been an Associate Editor for the IEEE Transactions on Image Processing and *Elsevier Signal Processing*.

Giuseppe Ruello (S'00–M'04) was born in Naples, Italy, on February 12, 1975. He received the Laurea degree (with honors) in telecommunication engineering and the Ph.D. degree in information engineering, in 1999 and 2003, respectively, both from the University of Naples Federico II, Naples, Itlaly.

In 2000, he received a grant from the University of Naples to be spent at the Department of Electronic and Telecommunication Engineering for research in the field of remote sensing. In 2000, he also won a grant from University of Rome La Sapienza, Rome, Italy. In 2002, as well as in 2004–2005, he was a Visiting Scientist with the Department of Signal Theory and Communications, Universitat Politecnica de Catalunya, Barcelona, Spain. Currently, he is a Research Scientist with the Department of Electrical and Information Technology Engineering, University of Naples. His research interests include SAR remote sensing, modeling of electromagnetic scattering from natural surfaces, SAR raw signal simulation, modeling of electromagnetic field propagation in urban environment, and remote sensing techniques for low-income semi-arid regions.

Luisa Verdoliva (M'13) received the Laurea degree in telecommunications engineering and the Ph.D. degree in information engineering from the University of Naples Federico II, Naples, Italy, in 1998 and 2002, respectively.

She is currently an Assistant Professor of Telecommunications with the University of Naples Federico II. Her research interests include image processing, in particular, compression and restoration of remote-sensing images, both optical and SAR, and digital forensics.

Dr. Verdoliva led the GRIP team of the University of Naples Federico II who ranked first in both the forgery detection and localization phases of the First Image Forensics Challenge organized in 2013 by the IEEE Information Forensics and Security Technical Committee (IFS-TC).

Giuseppe Scarpa (M'12) received the Laurea (M.S.) degree in telecommunication engineering and the Ph.D. degree in electronic and telecommunication engineering, both from the University of Naples Federico II, Naples, Italy, in 2001 and 2005, respectively.

Since 2006, he has been an Assistant Professor with the Department of Biomedical, Electronic, and Telecommunication Engineering, University of Naples Federico II. His research interests include image analysis and, in particular, segmentation, texture modeling and classification, object detection, and filtering, with applications in both remote sensing and medical domains.

Prof. Scarpa is currently an Associate Editor for IEEE Signal Processing Letters. In 2003, he was awarded a Marie Curie scholarship and was a Visiting Student at the INRIA Institute, France. Thanks to a joint ERCIM post-doctoral fellowship he was awarded in 2004, he has been a Research Fellow of both the UTIA Institute of the Czech Academy of Sciences, in 2005, and of the INRIA Institute, in 2006.